Reflectance of Silicon Photomultipliers at Vacuum Ultraviolet Wavelengths

P. Lv, G. F. Cao, L. J. Wen, S. Al Kharusi, G. Anton, I. J. Arnquist, I. Badhrees, P. S. Barbeau, D. Beck, V. Belov, T. Bhatta, P. A. Breur, J. P. Brodsky, E. Brown, T. Brunner, S. Byrne Mamahit, E. Caden, L. Cao, C. Chambers, B. Chana, S. A. Charlebois, M. Chiu, B. Cleveland, M. Coon, A. Craycraft, J. Dalmasson, T. Daniels, L. Darroch, A. De St. Croix, A. Der Mesrobian-Kabakian, K. Deslandes, R. DeVoe, M. L. Di Vacri, J. Dilling, Y. Y. Ding, M. J. Dolinski, L. Doria, A. Dragone, J. Echevers, F. Edaltafar, M. Elbeltagi, L. Fabris, D. Fairbank, W. Fairbank, J. Farine, S. Ferrara, S. Feyzbakhsh, A. Fucarino, G. Gallina, P. Gautam, G. Giacomini, D. Goeldi, R. Gornea, G. Gratta, E. V. Hansen, M. Heffner, E. W. Hoppe, J. Hößl, A. House, M. Hughes, A. Iverson, A. Jamil, M. J. Jewell, X. S. Jiang, A. Karelin, L. J. Kaufman, T. Koffas, R. Krücken, A. Kuchenkov, K. S. Kumar, Y. Lan, A. Larson, K. G. Leach, B. G. Lenardo, D. S. Leonard, G. Li, S. Li, Z. Li, C. Licciardi, R. MacLellan, N. Massacret, T. McElroy, M. Medina-Peregrina, T. Michel, B. Mong, D. C. Moore, K. Murray, P. Nakarmi, C. R. Natzke, R. J. Newby, Z. Ning, O. Njoya, F. Nolet, O. Nusair, K. Odgers, A. Odian, M. Oriunno, J. L. Orrell, G. S. Ortega, I. Ostrovskiy, C. T. Overman, S. Parent, A. Piepke, A. Pocar, J.-F. Pratte, V. Radeka, E. Raguzin, S. Rescia, F. Retière, M. Richman, A. Robinson, T. Rossignol, P. C. Rowson, N. Roy, J. Runge, R. Saldanha, S. Sangiorgio, K. Skarpaas VIII, A. K. Soma, G. St-Hilaire, V. Stekhanov, T. Stiegler, X. L. Sun, M. Tarka, J. Todd, T. I. Totev, R. Tsang, T. Tsang, F. Vachon, V. Veeraraghavan, S. Viel, G. Visser, C. Vivo-Vilches, J.-L. Vuilleumier, M. Wagenpfeil, T. Wager, M. Walent, Q. Wang, J. Watkins, W. Wei, U. Wichoski, S. X. Wu, W. H. Wu, X. Wu, Q. Xia, H. Yang, L. Yang, O. Zeldovich, J. Zhao, Y. Zhou, and T. Ziegler

***Abstract*— Characterization of the vacuum ultraviolet (VUV) reflectance of silicon photomultipliers (SiPMs) is important for large-scale SiPM-based photodetector systems. We report the angular dependence of the specular reflectance in vacuum of SiPMs manufactured by Fondazionc Bruno Kessler (FBK) and Hamamatsu Photonics K.K. (HPK) over wavelengths ranging from 120 to 280 nm. Refractive index and extinction coefficient of the thin silicon-dioxide film deposited on the surface of the FBK SiPMs are derived from reflectance data of an FBK silicon wafer with the same deposited oxide film as SiPMs. The diffuse reflectance of SiPMs is also measured at 193 nm. We use the VUV spectral dependence of the optical constants to predict the reflectance of the FBK silicon wafer and FBK SiPMs in liquid xenon.**

***Index Terms*— Diffuse reflectance, photon detection efficiency (PDE), silicon photomultiplier (SiPM), specular reflectance, vacuum ultraviolet (VUV).**

Manuscript received August 2, 2020; revised September 3, 2020; accepted October 27, 2020. Date of publication November 2, 2020; date of current version December 16, 2020. This work was supported in part by Chinese Academy of Sciences - Institute of High Energy Physics (CAS-IHEP) Fund for People's Republic of China (PRC)\U.S. Collaboration in High Energy Physics (HEP), in part by nEXO from the Office of Nuclear Physics of the Department of Energy and NSF in USA, in part by National Science and Engineering Research Council (NSERC), Canada Foundation for Innovation (CFI), Fonds de recherche Nature et technologies du Quebec (FRQNT), National Research Council (NRC), and the McDonald Institute (CFREF) in Canada, in part by Institute for Basic Sciences (Korea) (IBS) in South Korea, in part by Russian Foundation for Basic Research (RFBR) in Russia, under Grant 18-02-00550, and in part by CAS and NSFC in China.

Please see the Acknowledgment section of this article for the author affiliations.

Color versions of one or more figures in this article are available at https://doi.org/10.1109/TNS.2020.3035172.

Digital Object Identifier 10.1109/TNS.2020.3035172

I. Introduction

THE silicon photomultiplier (SiPM) is a novel solid-state silicon photon detector, composed of a dense array of single-photon avalanche diodes (SPADs) placed in parallel with a common anode and cathode [1]. Each SPAD is operated in Geiger mode and coupled with a quenching resistor. In recent decades, the vacuum ultraviolet (VUV) performance of SiPMs has been significantly improved, with reduced cost that warrants affordable meter-square-scale arrays of an SiPM photodetector system. Compared to traditional photomultiplier tubes (PMTs), SiPMs are more compact, have high radio purity, and exhibit good photon detection efficiency (PDE). These features make SiPMs more attractive for applications in cryogenic experiments, in particular, in rare-event searches [2]–[6]. There SiPMs benefit from applications in cryogenic environments that reduce the dark noise rate to the level of 1 Hz/mm^2 at liquid xenon (LXe) temperatures compared to rates of 50–100 kHz/mm^2 at room temperature [7]. The absolute PDE is a key performance parameter of SiPMs. It is related to the fraction of the sensor's sensitive area (fill factor), transmittance of SiPM surface layers, quantum efficiency (QE), and avalanche trigger probability. One way to improve the PDE is to design antireflective coatings (ARCs) on the SiPM surface to enhance the photon transmittance. In contrast to the visible region, the enhancement of the photon transmittance is particularly important for VUV wavelengths, where the refractive index of silicon is less than 1 [8]. For these wavelengths, the refractive index is much smaller than that of the intrinsic silicon dioxide (SiO_2) layer or other suitable ARC

materials. Over 50% of VUV photons can be reflected by the SiPM surface with a single layer of thin SiO_2, due to the large index mismatch. The reflection of photons is considered as a source of PDE loss during SiPM characterizations, because the PDE is usually measured with a single SiPM, where the reflected photons cannot be detected. However, in a large photodetector system, a fraction of reflected photons can be detected by other SiPMs and consequently the overall photon collection efficiency of the photodetector system becomes higher, compared with the one estimated by assuming no reflected photons being detected as the PDE measurement with a single SiPM. Here, the overall photon collection efficiency is defined as a ratio of the number of photons detected by the photodetector system to the number of photons originally generated. Knowledge on the VUV reflectance of SiPMs will allow us to better understand the optical response and the performance of SiPM photodetector systems. This has become an important R&D topic for large-scale photodetector programs [2], such as nEXO. The absolute PDE of SiPMs at VUV wavelengths is investigated in [9]–[12], however, little is known regarding the VUV reflectance of SiPMs.

The nEXO experiment is being designed to search for neutrinoless double beta decay in 5 tons of LXe enriched in the isotope ^{136}Xe in a time-projection chamber (TPC). Instead of the large-area APD used in detectors such as EXO-200 [13], a 4–5 m^2 SiPM array is proposed for the detection of the ~175 nm scintillation photons from LXe [2]. In combination with the information on charge detection in the TPC, the anticipated energy resolution is projected to be 1% at $Q_{\beta\beta}$ [14]. The overall PDE of the photodetector system is one of the major factors that will impact the energy resolution. The overall photon collection efficiency can be further classified into the photon transport efficiency (PTE) and PDE of SiPMs. The PTE can be quantified by a full Monte Carlo simulation with detailed geometry implementations and the knowledge of the optical properties of components inside the TPC. More details can be found in [14]. The VUV reflectance of SiPMs in LXe is one of the input parameters in such simulations conducted to accurately predict the PTE.

The nEXO collaboration has built a dedicated optical setup to study the reflectance of SiPMs in LXe, where SiPMs from HPK have been measured recently [15]. However, a vacuum-based setup has a wider VUV spectral range, and the reflectance in a vacuum (or argon- or nitrogen-purged setups) can guide us in verifying the results of LXe measurements. Establishing a predictable relationship between vacuum and LXe environments would be much more efficient and convenient than performing additional measurements in LXe, which are costly and complex. However, the direct prediction is complicated due to the diffuse component in the reflections, which is induced by the microstructure on SiPM's surface. The sufficient reflectance data, collected both in vacuum and in LXe, are critical to establish and validate this relationship. This article presents the measurement of SiPMs' reflectance in vacuum which provides an essential input for the direct comparison between measurements in vacuum and in LXe.

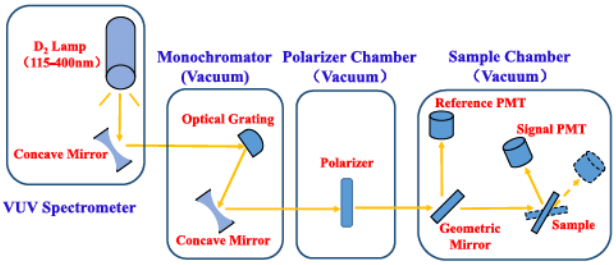

Fig. 1. Schematic of the specular reflection optical system. (From left to right: VUV spectrometer, monochromator chamber, polarization chamber, and sample chamber.)

This article is organized as follows. First, we discuss the instrumentation and sample characteristics. We quantify the measurement uncertainties. Then, we present the measurement results of VUV specular and diffuse reflectance. We derive the optical constants and the thickness of the SiO_2 film intrinsically deposited on the Fondazionc Bruno Kessler (FBK) SiPM surface. Finally, we use the VUV spectral dependence of the optical constants to predict the reflectance of the FBK silicon wafer and SiPMs in LXe.

II. Instrumentation

A. Specular Reflection Optical System

The VUV spectrophotometer of the specular reflection optical system is provided by Laser Zentrum Hannover, Germany, and its schematic is presented in Fig. 1. Two deuterium lamps with a magnesium fluoride (MgF_2) window and a quartz window serve as illuminants, which emit photons with wavelengths from 115 to 230 nm and from 170 to 300 nm, respectively. The spectral range can be selected during the measurement as long as the vacuum seal is not broken. The light beam is focused with a concave mirror onto the entry slit of a monochromator. The monochromator chamber contains an optical grating system used to select the wavelength and a second concave mirror to direct the irradiation into the sample chamber. The widths of the entrance slit and the exit slit are set at 100 μm, corresponding to a wavelength resolution of 0.8 nm. A polarization chamber can be inserted into the region between the monochromator chamber and the sample chamber to select incident light with a specific polarization. The sample chamber consists of a geometric mirror, a signal PMT with a UV-converter coating to detect reflected light, a reference PMT to monitor the stability of the light beam intensity and provide the intensity of incident light on samples based on the light intensity ratio between the signal PMT and the reference PMT, and movable units to rotate samples and the signal PMT. The incident angle onto the sample can be varied from 8° to 55° and it is automatically adjusted by software. The sample chamber is connected to a molecular pump, which can provide a 10^{-1} mbar vacuum for the whole system. The profile of the light beam is measured to be 3 mm × 5 mm, with the shape of a rectangle. After rotating the sample off the light beam, the intensity of the incident light for a given wavelength can be measured by the signal PMT.

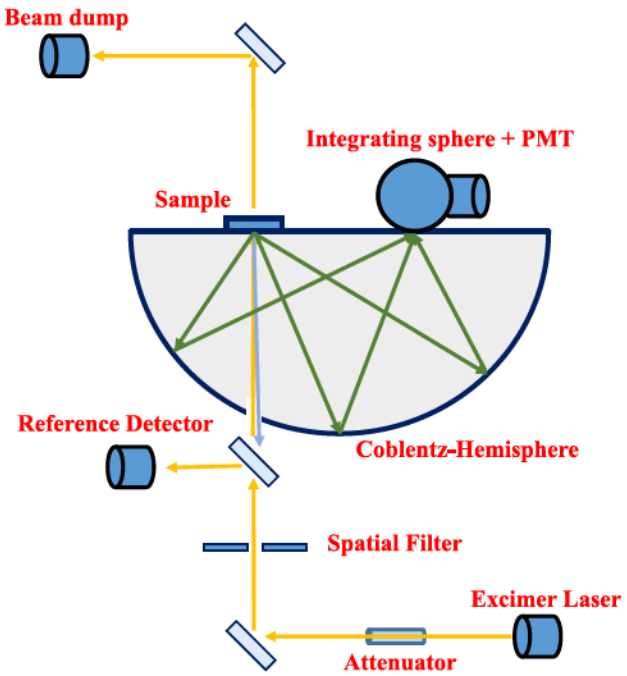

Fig. 2. Diagram of the TIS setup. (The yellow, blue, and green lines represent incident light, specular reflection light, and scattered light, respectively.)

The light intensity ratio between the signal PMT and the reference PMT is then obtained. Such procedure is repeated for different wavelengths. For one incidence angle, the signal PMT is rotated to search for the maximum intensity of the reflected light. The specular reflectance is obtained by dividing the maximum intensity of the reflected light and the intensity of the incident light. An aperture is placed in front of the signal PMT with a diameter of 4 mm. The distance between the sample and the signal PMT is 90 mm. Subsequently, the corresponding acceptance angle of the reflected light is calculated to be 1.55×10^{-3} radian.

B. Total Integrated Scatter Setup

The setup for the total integrated scatter (TIS) is manufactured by Laser Zentrum Hannover, the Department of Laser Components, according to ISO 13696:2002 [16]. The diagram of the setup is shown in Fig. 2, which is based on a Coblentz hemisphere with a diameter of 350 mm, designed to measure the low level of scatterings from the sample surfaces, even from optically smooth surfaces. The inner surface of the hemisphere is coated with an aluminum film and a protection layer to prevent aluminum oxidation. The aluminum film serves as a mirror and focuses light onto the detector. The light beam generated by a pulsed 193 nm laser is attenuated and guided onto the sample through the incident port, which has a diameter of 10 mm and an angle of incidence (AOI) close to 0°. Specular reflected light from the sample leave from the same port of incident light which has an open angle of 2×10^{-4} radian. Scattered light is collected by an integrating sphere with a UV-converter coating and then detected by a PMT attached to the sphere. The size of the light beam is 100 μm at the sample position, and the intensity of the light beam is monitored by a reference PMT via applying a beam splitter to the light beam. The sample to be measured sits on a 2-D transportation platform, which is used to scan the surface of the sample with a scan length of 50 mm in two directions. The resolution and repeatability of positioning are better than 100 and 200 μm, respectively. The detector and the sample to be measured are positioned at conjugate foci of the Coblentz hemisphere.

TABLE I
LIST OF MEASURED SAMPLES

Sample Name	Dimensions (mm × mm)	Pixel Size (μm)	Fill Factor
FBK-Si-Wafer #1	20 × 20	–	–
FBK-Si-Wafer #2	20 × 20	–	–
FBK-VUV-HD1-LF	10 × 10	30	73%
FBK-VUV-HD1-STD	10 × 10	30	73%
Hamamatsu-VUV4 #1	6 × 6	50	60%
Hamamatsu-VUV4 #2	6 × 6	75	70%

III. MEASURED SAMPLES

In this work, six samples are measured by a specular reflection optical system, and five of them are measured by the TIS. They are summarized in Table I. Four samples are provided by FBK. FBK-VUV-HD1-LF and FBK-VUV-HD1-STD are two types of VUV sensitive SiPMs developed in 2017 by FBK. These two FBK SiPMs have the same dimensions (10 mm × 10 mm), and the pixel size is 30 μm, which yields a fill factor of ~73%. To eliminate the influence on reflectance from the microstructure on the surface of SiPMs, FBK manufactured a 6-in silicon wafer deposited by a layer of SiO_2 with a thickness of approximately 1.5 μm. This silicon wafer is identical to the one used during SiPM manufacturing and diced into 20 mm × 20 mm pieces. Two of the pieces are selected to measure reflectance in this article. The remaining two samples are provided by HPK, which are the fourth-generation VUV-sensitive SiPMs (Hamamatsu-VUV4) with dimensions of 6 mm × 6 mm. The series numbers are S13370-6050CN and S13370-6075CN, corresponding to pixel sizes of 50 and 75 μm, respectively. The VUV4 SiPM with a larger pixel size has a larger fill factor.

IV. ESTIMATION OF MEASUREMENT UNCERTAINTIES

A blank silicon wafer is used as a reference sample to estimate uncertainties induced by the specular reflectance optical system. A native oxide layer, formed by the native oxidation process, exists on the surface of the reference sample, since the wafer has been exposed to air for a long time (more than 1 year). Thus, before the reference sample is delivered to the sample chamber, it undergoes three chemical cleaning processes, as discussed in [17], to remove the organic residuals, metal contamination, and native oxide layer on the wafer surface. However, after cleaning, a thin native oxide layer is still expected on the wafer surface, since the wafer has to be exposed to air while pumping the sample chamber (1–2 h). The thickness of the native oxide layer is approximately 1 nm based on studies in [18]. By assuming different thicknesses of the thin native oxide layer, the reflectance of

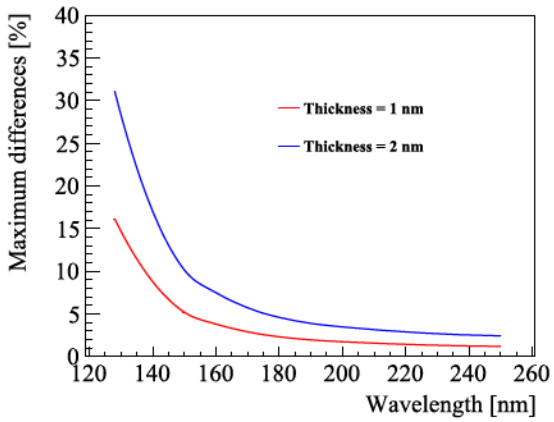

Fig. 3. Maximum differences in calculated reflectance over the full range of incident angles with thicknesses of 1 nm (red) and 2 nm (blue) of the oxide layer compared to that without the oxide layer as a function of wavelength.

the reference sample at different angles of incidence can be calculated based on Snell's law and Fresnel's equation (see more detailed discussions in Section V-C). Fig. 3 shows the calculated maximum percentage difference of the reflectance (over the full range of incident angles) between cases with and without the oxide layer for wavelengths from 120 to 250 nm. Oxide layer thicknesses of 1 and 2 nm were calculated and are presented as red and blue lines, respectively. At short wavelengths, the effect of the oxide layer on reflectance is much larger than that at longer wavelengths, and the thicker native oxide layer causes larger shifts in reflectance than those that occur in the case of no oxidation. Ratios of the measured reflectance and the calculated reflectance of the reference sample (assuming no oxide layer on the wafer) versus the AOI are shown in Fig. 4 for ten selected wavelengths. The results of s-polarization [Fig. 4(a)] and p-polarization [Fig. 4(b)] are compared separately. For wavelengths of 128 and 150 nm, larger discrepancies are observed since the reflectance is more sensitive to the thickness of the native oxide layer on the reference sample surface, however, information of the thickness is unknown to us. Thus, in uncertainty estimation, curves of 128 and 150 nm are excluded. For other wavelengths, the calculated results agree with the measurements within 8% (rel.) for both s-polarization and p-polarization, and we take this number as the systematic error induced by the specular reflectance optical system. Uncertainties from other factors are negligible.

The absolute uncertainty of the TIS is ±20%, as stated in its user manual. This uncertainty is dominated by unavailability of calibrated commercial samples and also arises from variations of the incident power and the beam diameter, variation of the signal processing system, and nonlinearity of the detector system. Even though a microroughened ceramic silicon carbide (SiC) sample, which shows an excellent long-term stability against VUV laser radiation, is taken as a diffuse reflecting standard and measured by a Perkin–Elmer spectrophotometer with an installed integral sphere to determine the total amount of diffuse reflectance, the environmental conditions between the two setups might be different. The relative uncertainty

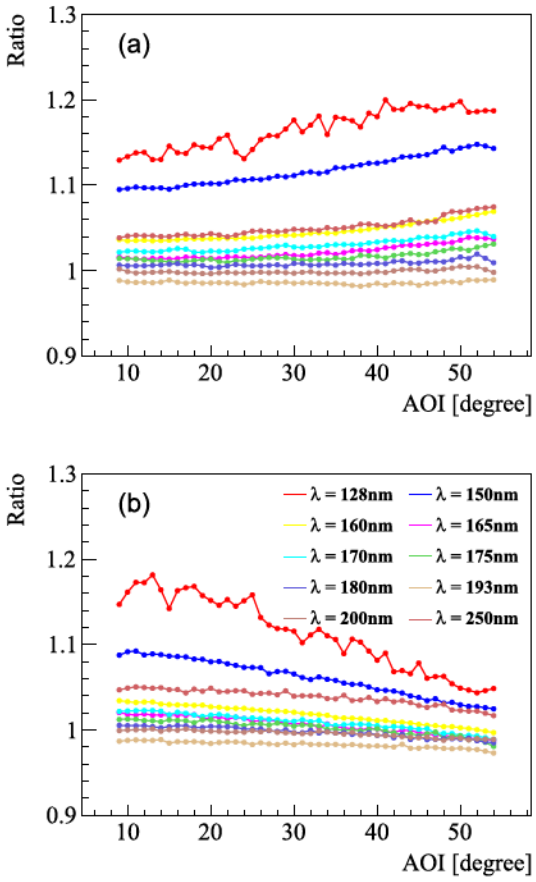

Fig. 4. Ratios of the measured reflectance and the calculated reflectance for the reference sample (assuming no oxide layer on the sample) as a function of AOI at ten different wavelengths: (a) s-polarization; (b) p-polarization.

of the TIS is ±5%, also quoted from the user manual, which means that the diffuse reflectance of different samples measured by the TIS setup can be compared with a relatively high accuracy.

V. Results

A. Specular Reflectance

The angular dependence of the specular reflectance is measured by the specular reflection optical system for the samples listed in Table I. Nine wavelengths are used in this measurement, covering the range from 128 to 200 nm. The results of four typical wavelengths are selected and shown in Fig. 5, in which 128 nm represents the central wavelength of scintillation light emitted from liquid argon [19], 175 nm is the peak of the LXe emission spectrum [20], and 193 nm is used in measuring the diffuse reflectance. The specular reflectance of five samples (FBK-Si-Wafer #2 is not shown) is measured with s-polarization (represented as solid lines) and p-polarization (represented as dashed lines) light separately. In general, the two FBK SiPM samples reflect more light at long wavelengths than the HPK SiPMs. However, at 128 nm, the trend is opposite for AOI less than 40°. The specular reflectance of the two VUV4 devices is found to decrease with the AOI. Data above 40° are not shown in the plots

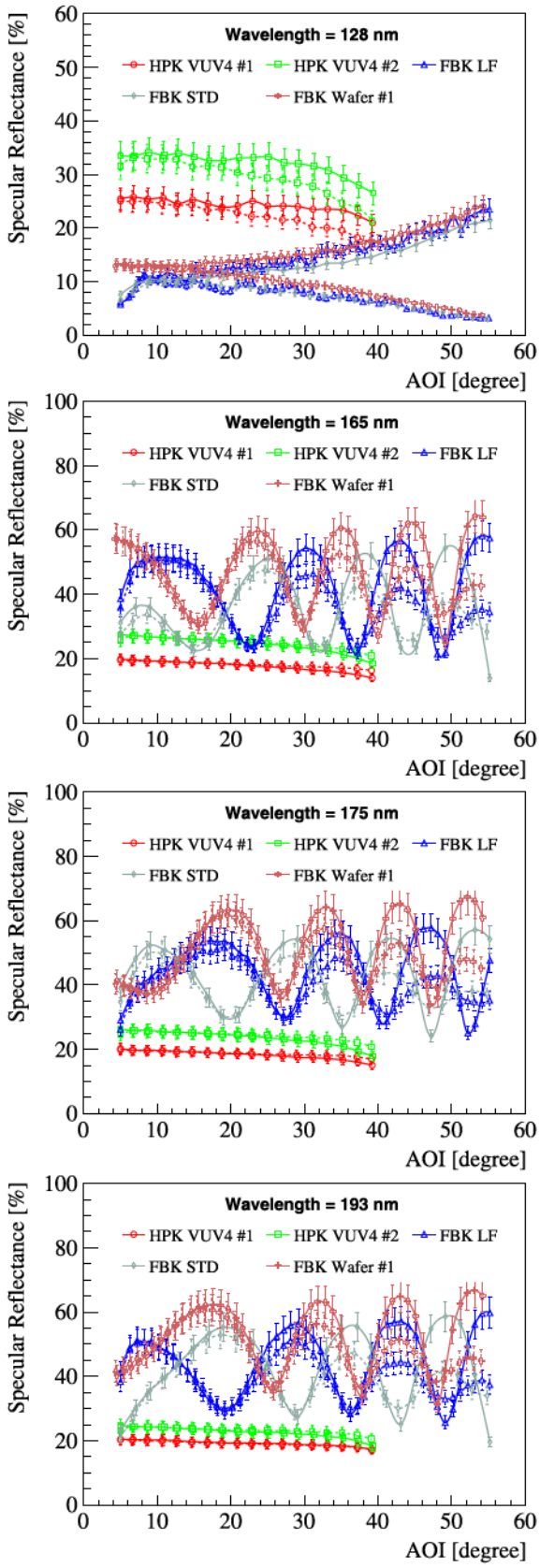

Fig. 5. Specular reflectance as a function of AOI for five samples measured at four wavelengths: 128, 165, 175, and 193 nm. The wavelength is labeled on each plot, and samples are indicated by different colors. Solid lines represent light beams with s-polarization, while dashed lines indicate p-polarization.

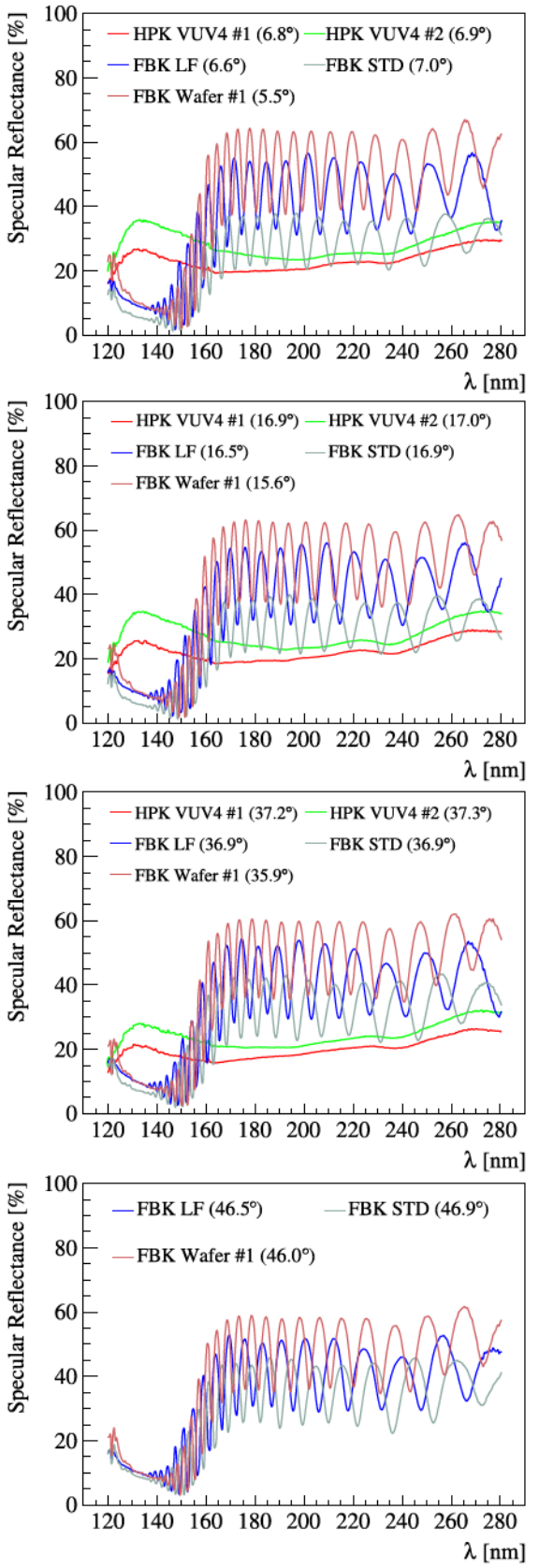

Fig. 6. Specular reflectance as a function of wavelengths for five samples measured at different incident angles, as indicated in the plots.

for the two HPK SiPMs because of shadowing effects of the sample holder. The sample holder is 1.5 mm higher than the sample surface, so part of the light is blocked at large incident angles. However, no such issue exists for the three FBK samples, because they have much larger dimensions. The sample of VUV4 #2 with the larger pixel size shows higher specular reflectance than that of VUV4 #1 due to its larger fill factor. The oscillation is not observed for HPK SiPMs but can clearly be seen in all three FBK samples at the three longer wavelengths. This result is caused by the interference of incident light in the thin SiO_2 layer deposited on the surface of the FBK samples. The thickness of the thin SiO_2 layer is approximately 1.5 μm, as measured by FBK [21]. The FBK-Si-Wafer sample has higher specular reflectance than that of the other two FBK SiPMs, because the microstructures on the surface of SiPMs, such as traces, quenching resistors, and so on, can reduce the specular reflectance. The FBK-VUV-HD1-LF and FBK-VUV-HD1-STD samples have almost the same reflectance, since they share similar profiles and surface structures. The shift of the oscillation phase between the two FBK SiPMs is introduced by the difference in the thickness of the SiO_2 layers on their surfaces.

Fig. 6 presents the specular reflectance versus different wavelengths for samples measured at different incident angles. The nonpolarized light beam is used in this measurement, and errors (rel. 8%) are omitted for clarity. The wavelength covers a range from 120 to 280 nm. Different samples are marked with different colors in the plots, together with their incident angles, which are indicated in brackets. Data at AOI of $\sim$46° are not drawn for the HPK SiPMs, due to the aforementioned shadowing effect. Similar to Fig. 5, the specular reflectance of the FBK samples oscillates with the wavelengths due to the interference induced by the thin SiO_2 layer. No oscillations are observed for the two HPK SiPMs. VUV4 #2 has larger specular reflectance in the range of measured wavelengths because of its larger fill factor. The specular reflectance of the two FBK SiPMs is slightly lower than that of the silicon wafer, as expected. The low reflectance of FBK-VUV-HD1-STD at selected incident angles compared with that of FBK-VUV-HD1-LF is caused by the different oscillation phases determined by the different thicknesses of the SiO_2 layer on the surfaces of the two samples.

B. Diffuse Reflectance

The diffuse reflectance of the five samples was measured using the TIS setup described in Section II-B. The TIS setup scanned each sample in vacuum to obtain the diffuse reflectance at different positions. The average diffuse reflectance within the inscribed circle of each sample is presented in Table II, where contributions from the specular reflected light, left from the entrance port on the TIS setup, are not included. The FBK silicon wafer shows a negligible amount of the diffuse component, due to its mirror-like surface. For SiPMs, a relatively large fraction of diffuse reflections are observed at a level of 10%. To compare the two SiPMs of HPK, the SiPM with the larger fill factor has lower diffusion, since the diffusion is mainly caused by the microstructure on the surface of the SiPM. For the two FBK SiPMs, the diffuse reflectance is similar to that of the HPK SiPMs. In addition to the amount of the absolute diffuse component, the angular response of diffuse reflections is also very interesting and an important input for detector simulation. The TIS setup does not have the ability to study this feature; instead, it will be studied in the future based on other ongoing setups.

TABLE II
RESULTS OF DIFFUSE REFLECTANCE FOR TWO FBK AND TWO HPK SIPMS. FOR COMPARISON, A SILICON WAFER FROM FBK HAS BEEN MEASURED AS A REFERENCE

Sample Name	Diffuse reflectance
FBK-Si-Wafer #1	(0.10 ± 0.02)%
FBK-VUV-HD1-LF	(10.0 ± 2.0)%
FBK-VUV-HD1-STD	(13.3 ± 2.7)%
Hamamatsu-VUV4 #1	(17.5 ± 3.5)%
Hamamatsu-VUV4 #2	(10.0 ± 2.0)%

C. Optical Properties of the SiO_2 Film

The optical properties of the ARC deposited on the SiPM surface possibly depend on the technologies used to produce the film. For the FBK SiPMs discussed in this work, a SiO_2 layer with the thickness of approximately 1.5 μm was deposited onto the silicon surfaces. The optical properties of the SiO_2 film, such as the refractive index (n) and extinction coefficient (k), can be extracted by analyzing the reflectance data of the FBK-Si-Wafer sample, because the SiO_2 films on the FBK-Si-Wafer and FBK SiPM were produced based on the same technologies, and almost no diffuse reflections occur on the FBK-Si-Wafer, which makes it easier to extract its n and k. For a two-media system, the reflection coefficient (the ratio of the electric field amplitudes of the incident light and reflected light) of light with s-polarization and p-polarization can be calculated by Fresnel's equation

$$r_s = \frac{\tilde{n}_0 \cos\theta_0 - \tilde{n}_1 \cos\theta_1}{\tilde{n}_0 \cos\theta_0 + \tilde{n}_1 \cos\theta_1} \quad r_p = \frac{\tilde{n}_1 \cos\theta_0 - \tilde{n}_0 \cos\theta_1}{\tilde{n}_0 \cos\theta_0 + \tilde{n}_1 \cos\theta_1} \tag{1}$$

in which $\tilde{n}_0$ and $\tilde{n}_1$ are complex indices of refraction of the first medium and the second medium, respectively, which are functions of the wavelength (λ) and can be expressed in terms of n and k:

$$\tilde{n} = n(\lambda) + ik(\lambda) \tag{2}$$

where θ_0 is the incident angle of the light beam and θ_1 the refractive angle. The relationship between θ_0 and θ_1 is determined by Snell's law

$$\tilde{n}_0 \sin(\theta_0) = \tilde{n}_1 \sin(\theta_1). \tag{3}$$

For the FBK-Si-Wafer sample, the SiO_2 film can be taken as a membrane; in this case, multiple reflections in the film will occur, and reflected light beams will interfere with each other. The total reflectance of light with s-polarization (R_s) and p-polarization (R_p) should be the superposition of all reflections. Based on (1) and (2), R_s and R_p can be easily

derived as

$$R_{\mathrm{s}} = |r_{\mathrm{s}}|^2 = \left| \frac{r_{s01} + e^{2i\delta} r_{s12}}{1 - e^{2i\delta} r_{s01} r_{s12}} \right|^2 \tag{4}$$

$$R_{\mathrm{p}} = |r_{\mathrm{p}}|^2 = \left| \frac{r_{p01} + e^{2i\delta} r_{p12}}{1 - e^{2i\delta} r_{p01} r_{p12}} \right|^2 \tag{5}$$

where $r_{\mathrm{s}01}$ ($r_{\mathrm{p}01}$) and $r_{\mathrm{s}12}$ ($r_{\mathrm{p}12}$) represent the reflection coefficients of light with s-polarization (p-polarization) from vacuum to SiO_2 and from SiO_2 to silicon, respectively. δ is the phase difference between two adjacent light beams, determined by

$$\delta = \frac{2\pi d_1}{\lambda} \tilde{n}_1 \cos\theta_1 \tag{6}$$

where d_1 denotes the thickness of the SiO_2 film, λ is the wavelength of the incident light, and $\tilde{n}_1$ and θ_1 are the complex refractive index and refractive angle in SiO_2, respectively. For nonpolarized light, the reflectance is an average of the reflectance of s-polarization and p-polarization

$$R = \frac{1}{2}(R_{\mathrm{S}} + R_{\mathrm{P}}). \tag{7}$$

For FBK-Si-Wafer #1 and FBK-Si-Wafer #2, the reflectance versus the AOI was measured at nine different wavelengths. The FBK-Si-Wafer #1 was measured by light with s-polarization and p-polarization separately and the #2 sample was measured with nonpolarized light. A customized fitting program is developed based on TMinuit [22] to simultaneously fit the reflectance data of FBK-Si-Wafer #1 and FBK-Si-Wafer #2 by using (7). Nonpolarized reflectance data (average of s-polarization and p-polarization for FBK-Si-Wafer #1) are used for both samples during the fitting. The n and k of silicon are from [8] and fixed in the fit. The n and k of SiO_2 and the two thicknesses of the two samples are the four floating parameters (assuming the thickness of SiO_2 film on one sample is uniform.). As examples, the fitted results at four wavelengths are shown in Fig. 7. The fitted curves reproduce well the measurements within the error bars. The systematic differences between the fitted curves and the data points for FBK-Si-Wafer #1 indicate that the quality of this data set is slightly worse. The amplitudes of reflectance of the two samples are identical within the uncertainty, and the phase differences in plots Fig. 7(b)-(d) are caused by the different thicknesses of oxide layers on the surfaces of the two samples. From the fitting, the average oxide-layer thicknesses of the #1 and #2 samples are found to be 1.519 ± 0.008 μm and 1.512 ± 0.008 μm, respectively. The oxide-layer thickness of sample #1 is also measured by an ellipsometer and determined to be 1.527 ± 0.004 μm, which agrees with the value determined in reflectance measurements. The maximum difference in oxide-layer thickness of sample #1 between the two measurements (rel. 1.5%) is taken as an uncertainty and added to the errors of the fitted n and k of SiO_2, which are shown in Fig. 8. The refractive index of the SiO_2 film from our measurements is slightly lower than the numbers measured in [23], as indicated by the black line, which might be a result of the different thickness of the film and manufacturing technologies used to make the film.

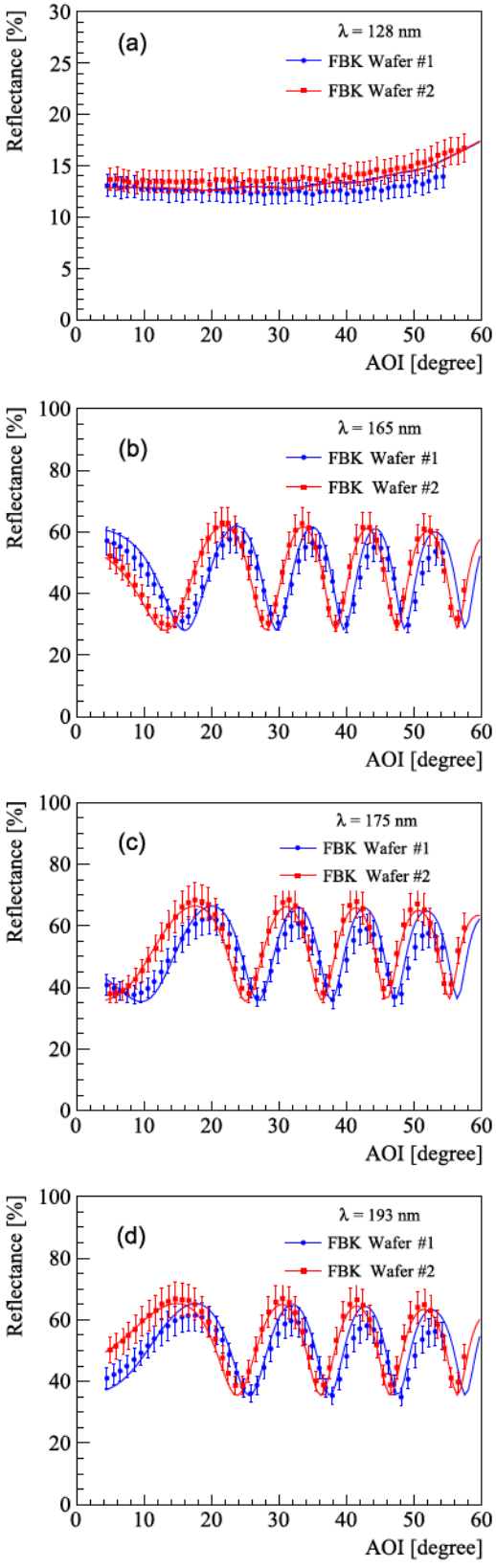

Fig. 7. Reflectance as a function of AOI measured at wavelengths of (a) 128 nm, (b) 165 nm, (c) 175 nm, and (d) 193 nm for the two FBK silicon wafer samples.

For the extinction coefficient of SiO_2, our data do not have good constraints at longer wavelengths, due to the very weak

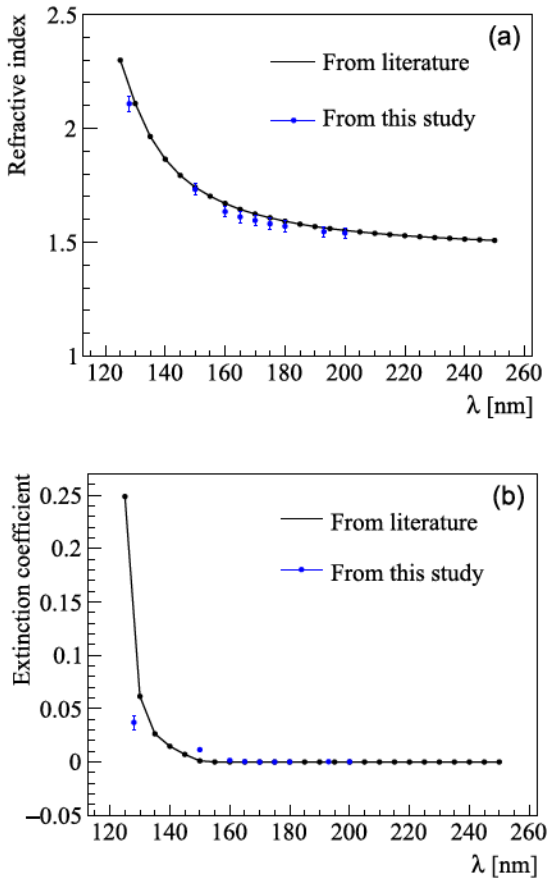

Fig. 8. (a) Fitted refractive index and (b) extinction coefficient of SiO_2 film, compared to results from the literature [23] (black lines).

absorption in the SiO_2 film. Moreover, the fitted values at short wavelengths do not match those in [23], as shown by the black line (see Fig. 8). This may be caused by the aforementioned reasons with that of the refractive index. The n and k of SiO_2 are calculated by fixing the thickness of the SiO_2 film of the two samples to above-average values in the fit.

D. Prediction of Reflectance in LXe

In the nEXO TPC, the SiPM array will be operated in LXe and thus an understanding of the reflectance of SiPMs in LXe is desired. Based on (7), the reflectance of the samples in LXe can be predicted based on the known composition and thickness and their refractive indices and extinction coefficients, in particular, for samples with a mirror-like surface. For SiPMs, this prediction becomes difficult due to the complex layout and materials of the microstructure on its surface, but for the specular reflection component, it should be possible. In this work, we calculate the reflectance of the FBK silicon wafer in LXe based on n and k of the SiO_2 film discussed in Section V-D and n of LXe reported in [24]. The results are shown in Fig. 9. The thickness of the SiO_2 layer on top of the silicon wafer is assumed to be 1.5 μm. Similar to that in a vacuum, the oscillation pattern caused by interference can be observed in LXe for incident light with a fixed wavelength, shown as the red curve in the figure. However, the amplitude of the oscillation is significantly suppressed

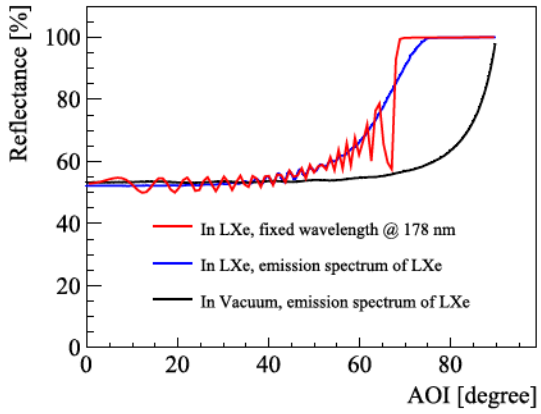

Fig. 9. Predicted reflectance as a function of AOI for the FBK silicon wafer. Red line: the reflectance in LXe for incident light with a fixed wavelength of 178 nm. Blue line: the reflectance in LXe for incident light with wavelengths that follow the distribution of the LXe emission spectrum. Black line: similar with the blue line, but calculated in vacuum.

in LXe. After taking the emission spectrum of LXe (central wavelength is 175 nm; full-width at half-maximum (FWHM) is 10 nm) [20] into account, the oscillation structure disappears both in vacuum and LXe, shown as the black curve and blue curve, respectively, because the effect of the interference is canceled out by the wavelength variation of the incident light. The critical angle in LXe becomes smaller than that in a vacuum; hence, total reflection can clearly be seen in LXe. The total reflection comes from the interface between the SiO_2 and the silicon, since n of silicon ($\sim$0.75) becomes much smaller than that of SiO_2 at 175 nm. The calculated reflectance of the FBK-Si-Wafer in LXe is (52.2 $\pm$ 1.6%) at the incident angle of 15°, which is consistent with the number of (50.8 $\pm$ 2.3%) measured at the same incident angle by the LXe-based setup in nEXO [15]. More comparisons at different incident angles will be performed in the near future. The specular reflectance of the measured FBK SiPMs in LXe can be roughly estimated by applying the same scale factor from vacuum to LXe, obtained from the FBK silicon wafer. For Hamamatsu SiPMs, their reflectance in LXe has to be measured by LXe-based setups, since we do not have any information on the ARC.

VI. Conclusion

We measured the specular and diffuse reflectance in a vacuum for the two FBK SiPMs (FBK-VUV-HD1-LF and FBK-VUV-HD1-STD) and two HPK SiPMs (VUV4 with a pixel size of 50 and 75 μm). The results show that SiPMs reflect a large fraction of VUV light. Furthermore, SiPMs from FBK are more reflective than those from HPK (VUV4). The diffuse component of reflective light is also observed, which is caused by the microstructures on the SiPM surface. The n and k of the SiO_2 film on the FBK silicon wafer are extracted by analyzing its reflectance data, which is an important input for the design of ARCs. Finally, the reflectance of the FBK silicon wafer in LXe is predicted based on the new n and k of the SiO_2 film and can be used to verify the output of LXe-based reflectance setups.

ACKNOWLEDGMENT

The authors would like to thank Dr. Cunding Liu from the Institute of Optics and Electronics, Chinese Academy of Sciences (CAS), and Prof. Bincheng Li from the University of Electronic Science and Technology of China for their substantial assistance with the reflectance setups.

P. Lv, L. J. Wen, Y. Y. Ding, X. S. Jiang, Z. Ning, X. L. Sun, W. Wei, W. H. Wu, and J. Zhao are with the Institute of High Energy Physics, Chinese Academy of Sciences, Beijing 100049, China.

G. F. Cao is with the Institute of High Energy Physics, Chinese Academy of Sciences, Beijing 100049, China, and also with the Department of Physics, University of Chinese Academy of Sciences, Beijing 100864, China (e-mail: caogf@ihep.ac.cn).

S. Al Kharusi, C. Chambers, L. Darroch, T. McElroy, M. Medina-Peregrina, K. Murray, and T. I. Totev are with the Physics Department, McGill University, Montréal, QC H3A 2T8, Canada.

G. Anton, J. Hößl, T. Michel, M. Wagenpfeil, and T. Ziegler are with the Erlangen Centre for Astroparticle Physics (ECAP), Friedrich-Alexander University Erlangen-Nürnberg, 91058 Erlangen, Germany.

I. J. Arnquist, M. L. Di Vacri, S. Ferrara, E. W. Hoppe, J. L. Orrell, G. S. Ortega, C. T. Overman, R. Saldanha, and R. Tsang are with the Pacific Northwest National Laboratory, Richland, WA 99352 USA.

I. Badhrees is with the Department of Physics, Carleton University, Ottawa, ON K1S 5B6, Canada, and also with the King Abdulaziz City for Science and Technology, Riyadh 12354, Saudi Arabia.

P. S. Barbeau and J. Runge are with the Department of Physics, Duke University, Durham, NC 27708 USA, and also with the Triangle Universities Nuclear Laboratory (TUNL), Durham, NC 27708 USA.

D. Beck, M. Coon, J. Echevers, and S. Li are with the Physics Department, University of Illinois, Urbana-Champaign, IL 61801 USA.

V. Belov, A. Karelin, A. Kuchenkov, V. Stekhanov, and O. Zeldovich are with the Institute for Theoretical and Experimental Physics named by A. I. Alikhanov of National Research Center "Kurchatov Institute," 117218 Moscow, Russia.

T. Bhatta, A. Larson, and R. MacLellan are with the Department of Physics, University of South Dakota, Vermillion, SD 57069 USA.

P. A. Breur, A. Dragone, L. J. Kaufman, B. Mong, A. Odian, M. Oriunno, P. C. Rowson, and K. Skarpaas VIII are with the SLAC National Accelerator Laboratory, Menlo Park, CA 94025 USA.

J. P. Brodsky, M. Heffner, A. House, S. Sangiorgio, and T. Stiegler are with the Lawrence Livermore National Laboratory, Livermore, CA 94550 USA.

E. Brown, A. Fucarino, and K. Odgers are with the Department of Physics, Applied Physics and Astronomy, Rensselaer Polytechnic Institute, Troy, NY 12180 USA.

T. Brunner is with TRIUMF, Vancouver, BC V6T 2A3, Canada, and also with the Physics Department, McGill University, Montréal, QC H3A 2T8, Canada.

S. Byrne Mamahit, F. Edaltafar, N. Massacret, and F. Retière are with TRIUMF, Vancouver, BC V6T 2A3, Canada.

E. Caden and B. Cleveland are with the Department of Physics, Laurentian University, Sudbury, ON P3E 2C6, Canada, and also with SNOLAB, Sudbury, ON P3Y 1N2, Canada.

L. Cao, Q. Wang, X. Wu, H. Yang, and Y. Zhou are with the Institute of Microelectronics, Chinese Academy of Sciences, Beijing 100029, China.

B. Chana, M. Elbeltagi, D. Goeldi, T. Koffas, S. Viel, C. Vivo-Vilches, and J. Watkins are with the Department of Physics, Carleton University, Ottawa, ON K1S 5B6, Canada.

S. A. Charlebois, K. Deslandes, F. Nolet, S. Parent, J.-F. Pratte, T. Rossignol, N. Roy, G. St-Hilaire, and F. Vachon are with the Département do génie électrique ot de génie informatique, Université de Sherbrooke, Sherbrooke, QC J1K 2R1, Canada.

M. Chiu, G. Giacomini, V. Radeka, E. Raguzin, S. Rescia, and T. Tsang are with the Brookhaven National Laboratory, Upton, NY 11973 USA.

A. Craycraft, D. Fairbank, W. Fairbank, A. Iverson, J. Todd, and T. Wager are with the Physics Department, Colorado State University, Fort Collins, CO 80523 USA.

J. Dalmasson, R. DeVoe, G. Gratta, M. J. Jewell, B. G. Lenardo, G. Li, and S. X. Wu are with the Physics Department, Stanford University, Stanford, CA 94305 USA.

T. Daniels is with the Department of Physics and Physical Oceanography, University of North Carolina at Wilmington, Wilmington, NC 28403 USA.

A. De St. Croix, G. Gallina, R. Krücken, and Y. Lan are with TRIUMF, Vancouver, BC V6T 2A3, Canada, and also with the Department of Physics and Astronomy, University of British Columbia, Vancouver, BC V6T 1Z1, Canada.

A. Der Mesrobian-Kabakian, J. Farine, C. Licciardi, A. Robinson, M. Walent, and U. Wichoski are with the Department of Physics, Laurentian University, Sudbury, ON P3E 2C6, Canada.

J. Dilling is with the Department of Physics and Astronomy, University of British Columbia, Vancouver, BC V6T 1Z1, Canada, and also with TRIUMF, Vancouver, BC V6T 2A3, Canada.

M. J. Dolinski, P. Gautam, E. V. Hansen, M. Richman, and A. K. Soma are with the Department of Physics, Drexel University, Philadelphia, PA 19104 USA.

L. Doria is with TRIUMF, Vancouver, BC V6T 2A3, Canada, and also with the Institut für Kernphysik, Johannes Gutenberg-Universität Mainz, 55122 Mainz, Germany.

L. Fabris and R. J. Newby are with the Oak Ridge National Laboratory, Oak Ridge, TN 37831 USA.

S. Feyzbakhsh, K. S. Kumar, A. Pocar, and M. Tarka are with the Amherst Center for Fundamental Interactions and Physics Department, University of Massachusetts, Amherst, MA 01003 USA.

R. Gornea is with TRIUMF, Vancouver, BC V6T 2A3, Canada, and also with the Department of Physics, Carleton University, Ottawa, ON K1S 5B6, Canada.

M. Hughes, P. Nakarmi, O. Nusair, I. Ostrovskiy, A. Piepke, and V. Veeraraghavan are with the Department of Physics and Astronomy, University of Alabama, Tuscaloosa, AL 35487 USA.

A. Jamil, Z. Li, D. C. Moore, and Q. Xia are with the Wright Laboratory, Department of Physics, Yale University, New Haven, CT 06511 USA.

K. G. Leach and C. R. Natzke are with the Department of Physics, Colorado School of Mines, Golden, CO 80401 USA.

D. S. Leonard is with the IBS Center for Underground Physics, Daejeon 34126, South Korea.

O. Njoya is with the Department of Physics and Astronomy, Stony Brook University, SUNY, Stony Brook, NY 11794 USA.

G. Visser is with the Department of Physics and CEEM, Indiana University, Bloomington, IN 47405 USA.

J.-L. Vuilleumier is with LHEP, Albert Einstein Center, University of Bern, 3012 Bern, Switzerland.

L. Yang is with the Physics Department, University of California, San Diego, CA 92093 USA.

REFERENCES

[1] D. Renker, "Geiger-mode avalanche photodiodes, history, properties and problems," *Nucl. Instrum. Meth. Phys. Res. A, Accel. Spectrom. Detect. Assoc. Equip.*, vol. 567, no. 1, pp. 48–56, Nov. 2006.

[2] n. Collaboration *et al.*, "NEXO pre-conceptual design report," 2018, *arXiv:1805.11142*. [Online]. Available: http://arxiv.org/abs/1805.11142

[3] R. Acciarri *et al.*, "Long-baseline neutrino facility (LBNF) and deep underground neutrino experiment (DUNE) conceptual design report, volume 4 the DUNE detectors at LBNF," 2016, *arXiv:1601.02984*. [Online]. Available: http://arxiv.org/abs/1601.02984

[4] A. M. Baldini *et al.*, "The design of the meg II experiment," *Eur. Phys. J. C*, vol. 78, no. 5, p. 380, May 2018.

[5] C. E. Aalsetch *et al.*, "Darkside-20k: A 20 tonne two-phase LAr TPC for direct dark matter detection at LNGS," *Eur. Phys. J. Plus*, vol. 133, p. 131, Mar. 2018.

[6] J. Aalbers *et al.*, "Darwin: Towards the ultimate dark matter detector," *J. Cosmology Astropart. Phys.*, vol. 2016, no. 11, p. 17, Jun. 2016.

[7] A. Gola *et al.*, "NUV-sensitive silicon photomultiplier technologies developed at fondazione bruno kessler," *Sensors*, vol. 19, no. 2, p. 308, Jan. 2019.

[8] H. R. Philipp and E. A. Taft, "Optical constants of silicon in the region 1 to 10 eV," *Phys. Rev.*, vol. 120, p. 37, Oct. 1960.

[9] I. Ostrovskiy *et al.*, "Characterization of silicon photomultipliers for nEXO," *IEEE Trans. Nucl. Sci.*, vol. 62, no. 4, pp. 1825–1836, Feb. 2015.

[10] A. Jamil *et al.*, "Vuv-sensitive silicon photomultipliers for xenon scintillation light detection in nexo," *IEEE Trans. Nucl. Sci.*, vol. 65, no. 11, p. 2823, Nov. 2018.

[11] G. Gallina *et al.*, "Characterization of the hamamatsu VUV4 MPPCs for nEXO," *Nucl. Instrum. Meth. Phys. Res. A, Accel. Spectrom. Detect. Assoc. Equip.*, vol. 940, pp. 371–379, Oct. 2019.

[12] K. Leki *et al.*, "Large-area mppc with enhanced VUV sensitivity for liquid xenon scintillation detector," *Nucl. Instrum. Meth. Phys. Res. A, Accel. Spectrom. Detect. Assoc. Equip.*, vol. 925, pp. 148–155, May 2019.

[13] M. Auger *et al.*, "The EXO-200 detector—Part I: Detector design and construction," *J. Instrum.*, vol. 7, no. 5, Feb. 2012, Art. no. 05010.
[14] J. B. Albert *et al.*, "Sensitivity and discovery potential of the proposed nEXO experiment to neutrinoless double-β decay," *Phys. Rev. C*, vol. 97, Jun. 2018, Art. no. 065503.
[15] P. Nakarmi *et al.*, "Reflectivity and PDE of VUV4 hamamatsu SiPMs in liquid xenon," *J. Instrum.*, vol. 15, no. 1, Jan. 2020, Art. no. P01019.
[16] *Optics and Optical Instruments—Test Methods for Radiation Scattered by Optical Components*. Standard ISO13696:2002, 1st ed, International Organization for Standardization, 2002.
[17] K. Wang *et al.*, "Chemical cleaning of silicon wafer surface," *Chin. J. Vac. Sci. Technol.*, vol. 4, pp. 322–326, Aug. 2007.
[18] M. Morita, T. Ohmi, E. Hasegawa, M. Kawakami, and M. Ohwada, "Growth of native oxide on a silicon surface," *J. Appl. Phys.*, vol. 68, pp. 1272–1281, Mar. 1990.
[19] T. Heindl *et al.*, "The scintillation of liquid argon," *Europhys. Lett.*, vol. 91, Sep. 2010, Art. no. 62002.
[20] K. Fujii *et al.*, "High-accuracy measurement of the emission spectrum of liquid xenon in the vacuum ultraviolet region," *Nucl. Instrum. Meth. Phys. Res. A, Accel. Spectrom. Detect. Assoc. Equip.*, vol. 795, p. 293, Sep. 2015.
[21] *Private Communications*, FBK, Italy, 2018.
[22] F. James. *Minuit Reference Manual*. Accessed: Mar. 27, 2019 [Online]. Available: https://root.cern.ch/download/minuit.pdf
[23] *Rochester Institute of Technology*. Accessed: Jan. 15, 2019. [Online]. Available: https://www.rit.edu/kgcoe/microsystems/lithography/thinfilms/cgi-bin/database.cgi?SiO2.csv
[24] V. N. Solotov *et al.*, "Measurement of the refractive index and attenuation length of liquid xenon for its scintillation light," *Nucl. Instrum. Meth. Phys. Res. A, Accel. Spectrom. Detect. Assoc. Equip.*, vol. 516, pp. 462–474, Jan. 2004.